

Drag and Entropy Variables

Carlos Lozano

Computational Aerodynamics Group

National Institute of Aerospace Technology (INTA)

Carretera de Ajalvir, km. 4. Torrejón de Ardoz, 28850, Spain

Abstract

Aerodynamic drag can be approximated by the entropy flux across fluid domain boundaries with a formula due to Oswatitsch. The adjoint solution that corresponds to this representation of the drag is investigated. For subcritical flows, the resulting adjoint variables are identical to the entropy variables, while for shocked flows there is a significant difference that is explicitly demonstrated with analytic solutions in the quasi-1D case. The approach is also investigated for 2D and 3D flows, where the adjoint equations and boundary conditions are derived. The approach is applied to mesh adaptation, performing comparably to the conventional near-field drag adjoint approach.

1. Introduction

Adjoint methods are routinely used in computational aerodynamics for shape design [1, 2] and error estimation and grid adaptation [3, 4] applications, among others. Adjoint states depend on both a base-line flow solution and an output function of the flow variables, in such a way that, for a given flow, there is a wide variety of adjoint solutions corresponding to different outputs. Typical output functions in aerodynamic applications are force (lift, drag, etc.) and moment coefficients, pressure distributions, flow input parameters (free-stream Mach number, flow direction), and combinations thereof.

This paper focuses on the adjoint solution corresponding to the entropy flux across domain boundaries. Since there is no entropy flux across solid walls, the above output measures the entropy balance across inlet/exit and far-field boundaries. This is of practical relevance since the boundary entropy balance is directly related to loss in turbomachines [5]. Likewise, as reviewed in section 2, under suitable assumptions aerodynamic drag can be approximated by the integrated entropy flux across far-field boundaries with a formula due to Oswatitsch [6]. In practice, other approaches for drag estimation that are indirectly based on the far-field entropy balance are used [7] besides conventional wall integration. These approaches allow for a clear separation of the different physical sources of drag and can be exploited in mesh adaptation [8].

Using entropy-based functionals is not new (see [9, 10] for general reviews on the use of entropy in numerical simulations). In [11], an adjoint-based shape design procedure for turbomachinery applications based on minimization of entropy losses was proposed, which however used the adjoint to a volume cost function measuring entropy production at boundary layers instead of the boundary entropy balance. Likewise, different forms of the residual of the entropy transport equation have been used as indicators for error estimation and grid adaptation in [12, 13, 14, 15, 16]. Along the same lines, it was pointed out in [17] that, for the Euler equations, the integrated entropy residual can be written as the residual of the flow equations weighted by the entropy variables [18, 19] and, likewise in shock-free cases, as the entropy flux across the domain boundaries. When shocks are present, the functional must include the shock loci as additional boundaries [20, 21, 22]. A similar relationship was established for the Navier-Stokes equations and was subsequently applied to drag error estimation and mesh adaptation via the Oswatitsch formula in [23]. The paper is organized as follows. Section 2 reviews the connection between entropy flux and aerodynamic drag. Section 3 addresses the far-field drag (Oswatitsch) adjoint for inviscid quasi-1D flow, where exact results can be derived, as well as for inviscid two- and three-dimensional (2D/3D) and laminar 2D flow. Section 4 presents numerical tests of the Oswatitsch-adjoint-based mesh adaptation approach, comparing it to the entropy adjoint and near-field drag adjoint approaches. Finally, section 5 contains a brief summary and discussion of the results.

2. Drag and entropy flux

Aerodynamic drag is the force exerted by a moving fluid on a solid body along the direction \vec{d} of the body's motion. For a body with a solid wall surface S_w immersed in a fluid domain with external (far-field) boundary S_∞ (Figure 1), drag can be computed as the integral of the fluid's momentum flux over the body surface. For inviscid flows, it reduces to

$$D_{near} = \int_{S_w} p \vec{d} \cdot \hat{n} dS \quad (1)$$

where \hat{n} is the outward-pointing unit normal vector and p is the pressure. Under suitable assumptions [23, 24], the contribution to eq. (1) due to shocks or boundary layers can be approximated by the entropy flux across the far-field boundary S_∞ with Oswatitsch's formula [6]:

$$D_{osw} \approx -\frac{\vec{u}_\infty \cdot \vec{d}}{\gamma M_\infty^2} \int_{S_\infty} \vec{\Phi} \cdot \hat{n} dS \quad (2)$$

where $\vec{\Phi} = -\rho s \vec{u} / R$ is the entropy flux, ρ and \vec{u} are the fluid's density and velocity, respectively, $s = R \log(p / \rho^\gamma) / (\gamma - 1)$ is the entropy, R the gas constant, γ the adiabatic exponent, \vec{u}_∞ the velocity of the incoming flow (free-stream velocity) and M_∞ the free-stream Mach number.

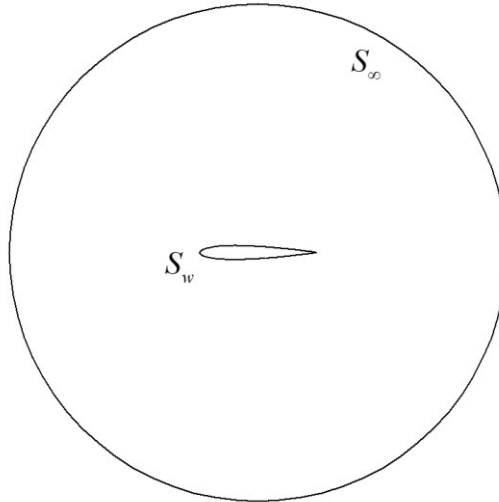


Figure 1: Sketch of a typical 2D flow configuration.

3. The Oswatitsch adjoint

We will now analyze the adjoint solution corresponding to the entropy flux across the fluid domain outer boundaries. As a warm-up we will start with quasi-1D inviscid flow (for which exact results for both the flow and the adjoint equations can be derived) and then proceed to the more engineeringly relevant 2D and 3D cases.

3.1. Quasi-one-dimensional inviscid flow

The (steady) quasi-one-dimensional Euler equations in a duct of cross-section $A(x)$ with $-1 \leq x \leq 1$ read

$$R(U, A) = \frac{d}{dx}(AF) - \frac{dA}{dx}P = 0, \quad (3)$$

where

$$U = \begin{pmatrix} \rho \\ \rho u \\ \rho E \end{pmatrix}, \quad F = \begin{pmatrix} \rho u \\ \rho u^2 + p \\ \rho u H \end{pmatrix}, \quad P = \begin{pmatrix} 0 \\ p \\ 0 \end{pmatrix} \quad (4)$$

and

$$p = (\gamma - 1)\rho \left(E - \frac{1}{2}u^2 \right), \quad H = E + \frac{p}{\rho} = \frac{\gamma}{\gamma - 1} \frac{p}{\rho} + \frac{1}{2}u^2 \quad (5)$$

Here u is the velocity, while E and H are the total energy and enthalpy, respectively. Eq. (3) holds for shock-free flows. If the solution contains a shock at x_s , Eq. (3) holds on either side of the shock, and matching across the shock is provided by the Rankine-Hugoniot jump condition $[F]_{x_s^\pm} = 0$. Away from shocks, entropy is conserved. Letting $\Phi = -\rho u s / R$ denote the entropy flux, entropy conservation is encoded in the equation $d(A\Phi) / dx = 0$. Focusing on the entropy balance through the inlet/exit boundaries, we choose the following cost function

$$J = [A\Phi]_{-1}^{+1} \quad (6)$$

(i.e. the net entropy flux across the duct's ends). The adjoint construction for smooth flows requires one adjoint state $\psi = (\psi_0, \psi_1, \psi_2)^T$ to enforce the flow equations in the Lagrangian

$$J = [A\Phi]_{-1}^{+1} - \int_{-1}^{+1} \psi^T R(U, A) dx \quad (7)$$

Linearizing (7) with respect to A and U , integrating by parts and rearranging yields

$$\delta J = [\delta A\Phi]_{-1}^{+1} + \int_{-1}^{+1} \psi^T \left[\frac{d\delta A}{dx} P - \frac{d}{dx} (\delta A F) \right] dx \quad (8)$$

which is independent of δU , provided that ψ obeys the adjoint equation

$$-AF_U^T \frac{d\psi}{dx} - \frac{dA}{dx} P_U^T \psi = 0, \quad (9)$$

with the inlet/exit boundary conditions

$$(v - \psi)^T F_U \delta U \Big|_{x=\pm 1} = 0 \quad (10)$$

where

$$v^T = -\frac{\partial}{\partial U} (\rho s / R) = \left(\frac{\gamma}{\gamma - 1} - \frac{s}{R} - \frac{\rho u^2}{2p}, \frac{\rho u}{p}, -\frac{\rho}{p} \right) \quad (11)$$

are the entropy variables, which obey the compatibility condition $\Phi_U = v^T F_U$. In the shock-free case, it can be shown that equations (9) and (10) imply that $\psi = v$, i.e., the entropy variables are adjoint to the net entropy flux as first pointed out in [17]. If there is a shock at x_s , the linearization now includes the linear perturbation in the shock position, δx_s [25]. The adjoint construction requires two adjoint states ψ, ϕ to enforce the flow and Rankine-Hugoniot equations, resulting in the Lagrangian

$$J = [A\Phi]_{-1}^{+1} - \int_{-1}^{x_s^-} \psi^T R(U, A) dx - \int_{x_s^+}^{+1} \psi^T R(U, A) dx - A_s \phi^T [F]_{x_s^\pm} \quad (12)$$

where $A_s = A(x_s)$. Linearizing with respect to A , U and x_s , integrating by parts and rearranging yields

$$\delta J = [\delta A\Phi]_{-1}^{+1} + \int_{-1}^{x_s^-} \psi^T \left[\frac{d\delta A}{dx} P - \frac{d}{dx} (\delta AF) \right] dx + \int_{x_s^+}^{+1} \psi^T \left[\frac{d\delta A}{dx} P - \frac{d}{dx} (\delta AF) \right] dx \quad (13)$$

independently of δU and δx_s , provided that $\varphi = 0$ and ψ obeys the adjoint equation (9) on either side of the shock with inlet/exit boundary conditions (10), as well as an internal shock boundary condition

$$\psi^T F_U \delta U \Big|_{x_s^+} - \psi^T F_U \delta U \Big|_{x_s^-} = 0 \quad (14)$$

It can be shown [21] that (14) requires that the adjoint variables be continuous at the shock with zero derivative and obey the internal boundary condition $\psi_1(x_s) = 0$. The above equations are incompatible with ψ being the entropy variables, which are discontinuous at the shock. In fact, the entropy variables are adjoint to the cost function $[A\Phi]_{-1}^{+1} - [A\Phi]_{x_s^-}^{x_s^+}$ measuring the net entropy balance across the domain boundaries and flow discontinuities (including the shock) [20, 21].

For given flow conditions and area distribution $A(x)$, the analytic solution to the quasi-1D equations can be obtained with the Area-Mach number relation [26], while the corresponding adjoint solution, for arbitrary choices of the functional, can be obtained with the Green's function approach of [25]. This exercise can be carried out for a converging-diverging symmetric duct with cross section

$$A(x) = \begin{cases} 2, & |x| > 0.5 \\ 1 + \sin^2 \pi x, & |x| \leq 0.5 \end{cases}$$

and transonic flow conditions which result in a sonic throat at $x = 0$ and a shock at $x_s \approx 0.152$. The analytic entropy variables can be obtained from the flow solution using (11), while a closed-form expression for the Oswatitsch adjoint variables has been obtained in [21]. Both sets of variables are compared in Figure 2 for the shocked case, as well as for a subsonic case with $M_m = 0.2$. In the subsonic case, the Oswatitsch adjoint variables are identical to the entropy variables, while for the shocked case there is a significant difference. While entropy variables are continuous at the sonic throat and discontinuous at the shock, Oswatitsch adjoint variables are continuous at the shock with zero gradient but show a finite jump at the sonic throat.

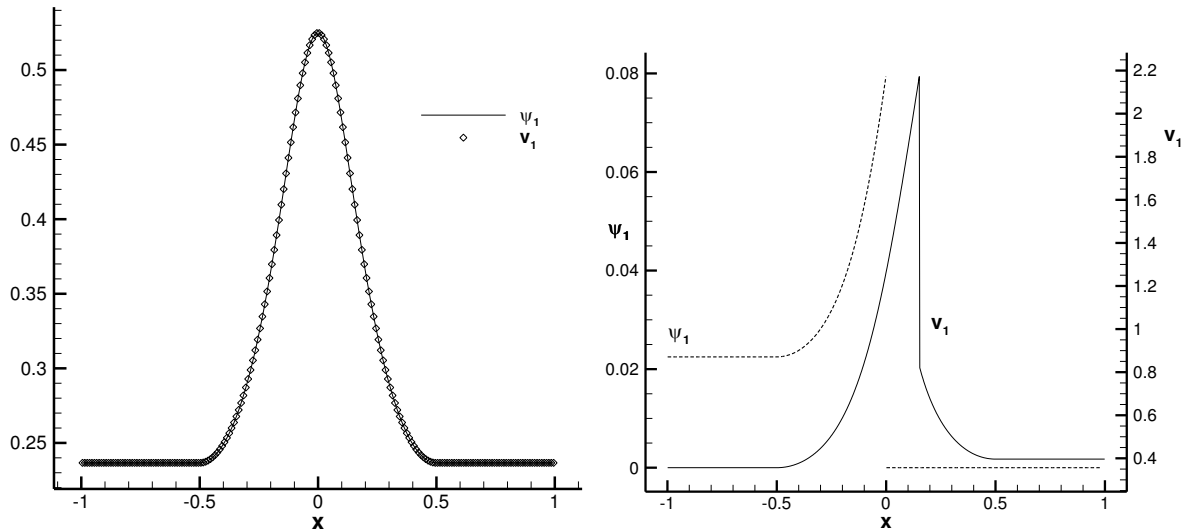


Figure 2: Entropy variables and Oswatitsch adjoint for subsonic (left) and shocked (right) flow conditions.

3.2 Two-dimensional inviscid flow

Let us now move on to two dimensions. We assume that the fluid domain Ω has a boundary $\partial\Omega$ formed by a solid wall S_w and a far field boundary S_∞ , as depicted in Figure 1. The flow obeys the (steady) Euler equations

$$R(U) = \nabla \cdot \vec{F}(U) = 0, \quad (15)$$

where

$$U = \begin{pmatrix} \rho \\ \rho u_1 \\ \rho u_2 \\ \rho E \end{pmatrix}, \quad \vec{F} = \begin{pmatrix} \rho \vec{u} \\ \rho \vec{u} u_1 + p \hat{x} \\ \rho \vec{u} u_2 + p \hat{y} \\ \rho \vec{u} H \end{pmatrix} \quad (16)$$

In these definitions, u_1, u_2 are the Cartesian components of the velocity vector \vec{u} . The flow equations are supplemented with non-transpiration conditions $\vec{u} \cdot \hat{n} = 0$ on S_w and characteristic boundary conditions on S_∞ . If the solution U contains a shock along a curve Σ , the Rankine-Hugoniot jump condition $[\vec{F}] \cdot \hat{n}_\Sigma = 0$ connects the smooth solutions $R(U) = 0$ on either side. Here $[\vec{F}] = \vec{F}|_{\text{downstream}} - \vec{F}|_{\text{upstream}}$ denotes the jump in \vec{F} across the shock and \hat{n}_Σ is the unit normal vector to Σ oriented such that it points upstream of the shock –see Figure 3. The cost function is again the entropy flux across the domain boundaries

$$J = \int_{\partial\Omega} \vec{\Phi} \cdot \hat{n} dS = -\frac{1}{R} \int_{\partial\Omega} \rho s \vec{u} \cdot \hat{n} dS = -\frac{1}{R} \int_{S_\infty} \rho s \vec{u} \cdot \hat{n} dS \quad (17)$$

For subsonic conditions (such that the flow remains smooth throughout the domain) deriving the adjoint equations requires an adjoint state $\psi = (\psi_0, \psi_1, \psi_2, \psi_3)^T$ to enforce the flow equations on (17),

$$J = \int_{S_\infty} \vec{\Phi} \cdot \hat{n} dS - \int_{\Omega} \psi^T \nabla \cdot \vec{F}(U) d\Omega \quad (18)$$

Linearizing (18) with respect to U , integrating by parts and rearranging yields

$$\begin{aligned} \delta J = & \int_{S_\infty} \vec{\Phi}_U \cdot \hat{n} \delta U dS + \int_{\Omega} \nabla \psi^T \cdot \vec{F}_U \delta U d\Omega - \int_{S_\infty} \psi^T \hat{n} \cdot \vec{F}_U \delta U dS - \int_{S_w} \psi^T \hat{n} \cdot \vec{F}_U \delta U dS = \\ & - \int_{S_w} \rho \delta \vec{u} \cdot \hat{n} (\psi_0 + \vec{\varphi} \cdot \vec{u} + \psi_3 H) dS + \int_{\Omega} \nabla \psi^T \cdot \vec{F}_U \delta U d\Omega + \int_{S_\infty} (\mathbf{v} - \psi)^T \vec{F}_U \cdot \hat{n} \delta U dS - \int_{S_w} (\vec{\varphi} \cdot \hat{n}) \delta p dS \end{aligned} \quad (19)$$

where $\vec{\varphi} = (\psi_1, \psi_2)$ is the adjoint momentum vector and

$$\mathbf{v}^T = -\frac{\partial}{\partial U} (\rho s / R) = \left(\frac{\gamma}{\gamma-1} - \frac{s}{R} - \frac{\rho \vec{u}^2}{2p}, \frac{\rho \vec{u}}{p}, -\frac{\rho}{p} \right) \quad (20)$$

are the entropy variables. Since $\delta \vec{u} \cdot \hat{n}$ on S_w can be written in terms of known quantities using the linearized wall boundary condition $\delta(\vec{u} \cdot \hat{n}) = \delta \vec{v} \cdot \hat{n} + (\delta \vec{x}_{S_w} \cdot \nabla) \vec{u} \cdot \hat{n} + \vec{u} \cdot \delta \hat{n}$ (here $\delta \vec{x}_{S_w}$ is the wall boundary deformation that appears in shape design applications), independence of (19) from δU requires that ψ obeys the adjoint equation

$$\nabla \psi^T \cdot \vec{F}_U = 0 \quad (21)$$

with boundary conditions

$$\begin{aligned} (\mathbf{v} - \boldsymbol{\psi})^T (\vec{F}_U \cdot \hat{\mathbf{n}}) \delta U \Big|_{s_w} &= 0, \\ \vec{\varphi} \cdot \hat{\mathbf{n}} \Big|_{s_w} &= 0. \end{aligned} \quad (22)$$

As in the quasi-1D case, (21)-(22) require that $\boldsymbol{\psi} = \mathbf{v}$, so the entropy variables are, again, adjoint to the cost function (17). When (21)-(22) hold, the linear perturbation of J can be computed by the remaining terms of (19) as

$$\delta J = - \int_{s_w} \rho \delta \bar{\mathbf{u}} \cdot \hat{\mathbf{n}} (\psi_0 + \vec{\varphi} \cdot \bar{\mathbf{u}} + \psi_3 H) dS \quad (23)$$

which can be applied, for example, to compute gradients of the cost function with respect to variations in the shape of S_w in the context of adjoint-based shape design.

When shocks are present, the above analysis needs to be modified to account for the perturbation in the shock strength and position. A detailed adjoint analysis for shocked 2D cases has been carried out in [27] (see also [21]) for a functional consisting on a function of the pressure integrated along the wall and can be easily adapted to the present case as follows. If the flow is perturbed by a small change in boundary or flow conditions, a deformation of the solid wall, errors or uncertainties in the solution, etc., the shock structure and position will be different, and we will assume that the new shock curve can be described in terms of a local (small) deformation $\bar{x}_\Sigma \rightarrow \bar{x}_\Sigma + \delta \bar{x}_\Sigma$. The perturbations in the flow δU and shock position $\delta \bar{x}_\Sigma$ can be obtained from the linearized flow and Rankine-Hugoniot equations,

$$\begin{aligned} \nabla \cdot (\vec{F}_U \delta U) &= 0 \quad \text{in } \Omega \setminus \Sigma \\ [\vec{F}_U \delta U]_\Sigma \cdot \hat{\mathbf{n}}_\Sigma + [\vec{F} \cdot \delta \hat{\mathbf{n}}_\Sigma]_\Sigma + [(\delta \bar{x}_\Sigma \cdot \nabla) \vec{F} \cdot \hat{\mathbf{n}}_\Sigma]_\Sigma &= 0 \quad \text{on } \Sigma \end{aligned} \quad (24)$$

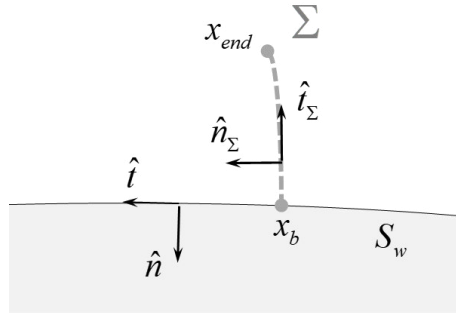


Figure 3: Schematics of shock location and conventions. Flow direction is from left to right.

Introducing adjoint states $\boldsymbol{\psi}$ and $\boldsymbol{\psi}_s$ to enforce the flow and shock equations, the linearized perturbation to the cost function (17) can be written as

$$\delta J = \int_{s_w} \vec{\Phi}_U \cdot \hat{\mathbf{n}} \delta U dS - \int_{\Omega \setminus \Sigma} \boldsymbol{\psi}^T \nabla \cdot (\vec{F}_U \delta U) d\Omega - \int_{\Sigma} \boldsymbol{\psi}_s^T \left([\vec{F}_U \delta U]_\Sigma \cdot \hat{\mathbf{n}}_\Sigma + [\vec{F} \cdot \delta \hat{\mathbf{n}}_\Sigma]_\Sigma + [(\delta \bar{x}_\Sigma \cdot \nabla) \vec{F} \cdot \hat{\mathbf{n}}_\Sigma]_\Sigma \right) d\Sigma \quad (25)$$

The manipulation of Eq. (25) involves three basic steps (further details can be found in [21]): integrating by parts the field integral, separating $\delta \bar{x}_\Sigma = \delta \Sigma_t \hat{\mathbf{t}}_\Sigma + \delta \Sigma_n \hat{\mathbf{n}}_\Sigma$ into its tangent and normal components, and integrating by parts along Σ the resulting tangent derivatives $\partial_{t_g} = \hat{\mathbf{t}}_\Sigma \cdot \nabla$. This yields

$$\begin{aligned} \delta J &= - \int_{s_w \setminus x_b} \rho \delta \bar{\mathbf{u}} \cdot \hat{\mathbf{n}} (\psi_0 + \vec{\varphi} \cdot \bar{\mathbf{u}} + \psi_3 H) dS + \int_{\Omega \setminus \Sigma} \nabla \boldsymbol{\psi}^T \cdot \vec{F}_U \delta U d\Omega + \int_{s_w} (\mathbf{v} - \boldsymbol{\psi})^T \vec{F}_U \cdot \hat{\mathbf{n}} \delta U dS - \int_{s_w \setminus x_b} (\vec{\varphi} \cdot \hat{\mathbf{n}}) \delta p dS \\ &\quad - \int_{\Sigma} [(\boldsymbol{\psi} + \boldsymbol{\psi}_s)^T \vec{F}_U \delta U]_\Sigma \cdot \hat{\mathbf{n}}_\Sigma d\Sigma - \int_{\Sigma} \partial_{t_g} \boldsymbol{\psi}_s^T [\vec{F} \cdot \hat{\mathbf{t}}_\Sigma]_\Sigma \delta \Sigma_n d\Sigma - \boldsymbol{\psi}_s^T [\vec{F} \cdot \hat{\mathbf{t}}_\Sigma]_\Sigma \delta \Sigma_n \Big|_{x_b} \end{aligned} \quad (26)$$

Eq. (26) can be computed by the first term on the right-hand side (and thus independently of δU and $\delta \bar{x}_\Sigma$) if $\boldsymbol{\psi}$ obeys the adjoint equation (21) and wall and far-field boundary conditions (22). At the shock, $\boldsymbol{\psi}$ and $\boldsymbol{\psi}_s$ must be related such that $\boldsymbol{\psi} \Big|_{\Sigma^{sup}} = -\boldsymbol{\psi}_s = \boldsymbol{\psi} \Big|_{\Sigma^{down}}$, so $\boldsymbol{\psi}$ must be continuous across the shock. Eq. (26) also requires

$$\partial_{t_g} \psi^T [\vec{F} \cdot \vec{t}_\Sigma]_\Sigma = 0 \quad (27)$$

which is a differential equation along the shock, and

$$\psi^T(x_b) [\vec{F} \cdot \vec{t}_\Sigma]_{x_b} = 0 \quad (28)$$

at the shock root x_b , where $[\]_{x_b}$ is the jump across the shock at the shock root. Using the shock equations (27) and (28), it can be shown [21] that for normal shocks, for example, adjoint normal derivatives are mostly vanishing (and continuous) across the shock. At any rate, these equations are usually not taken into account for the discretization of the adjoint equations. It is assumed that the discrete adjoint system picks the correct solution satisfying (27) and (28) provided that there is enough dissipation across the shock [28]. However, taking the shock relations into account does have an impact in shape optimization [27].

A final comment concerns the relation of the Oswatitsch adjoint to the entropy variables in the shocked case. Entropy variables are necessarily discontinuous at shocks, so they cannot obey the above equations. Hence, for shocked flows, as in the quasi-1D case, the Oswatitsch adjoint differs from the entropy variables, which are in fact adjoint to the cost function

$$\int_{\Omega \cup \Sigma} v^T R(U) d\Omega = \int_{\Omega \cup \Sigma} \nabla \cdot \left(-\frac{\rho \vec{u} s}{R} \right) d\Omega = -\frac{1}{R} \int_{S_w} \rho \vec{u} \cdot \hat{n} dS - \frac{1}{R} \int_{\Sigma} [\rho \vec{u}]_{\Sigma} \cdot \hat{n}_{\Sigma} d\Sigma \quad (29)$$

3.3 Two-dimensional viscous flow

The Oswatitsch formula can be also applied to viscous flows. As above, it is possible to derive the adjoint scheme in this case. Adjoint analysis for viscous flows are quite standard now (see for example [29, 30, 31, 32]) and we will not go through the derivation here. We will just state the basic results. If the (steady) Navier-Stokes equations are written as

$$\nabla \cdot (\vec{F} - \vec{F}^v) = \nabla \cdot \vec{F} - \nabla \cdot (\mathbf{K} \cdot \nabla U) = 0 \quad (30)$$

where $\vec{F}^v = \mathbf{K} \cdot \nabla U$ are the viscous fluxes, then the adjoint state $\psi = (\psi_0, \psi_1, \psi_2, \psi_3)^T$ that corresponds to (17) obeys the adjoint equation

$$\vec{F}_U^T \cdot \nabla \psi - \nabla U^T \cdot \frac{\partial \mathbf{K}^T}{\partial U} \cdot \nabla \psi + \nabla \cdot (\mathbf{K}^T \cdot \nabla \psi) = 0 \quad (31)$$

with boundary conditions

$$\begin{aligned} (\mathbf{v} - \psi)^T (\vec{F}_U \cdot \hat{n}) \delta U \Big|_{S_w} &= 0, \\ \vec{\varphi} \Big|_{S_w} &= (\psi_1, \psi_2) \Big|_{S_w} = 0, \\ \partial_n \psi_3 \Big|_{S_w} &= 0 \end{aligned} \quad (32)$$

where adiabatic boundary conditions $\partial_n T \Big|_{S_w} = 0$ have been assumed for the primal flow at the wall.

The situation with entropy variables is different in this case [17]. It turns out that entropy variables are no longer adjoint variables (i.e., they do not obey eq. (31) but a closely related one) and they are not related to the entropy flux but to the viscous entropy residual

$$J = -\frac{1}{R} \int_{\Omega} \left(\nabla \cdot (\rho \vec{u} s) - \frac{1}{T} (\sigma : \nabla u + \nabla \cdot (k \nabla T)) \right) d\Omega = \int_{\partial \Omega} \vec{\Phi} \cdot \hat{n} dS + \int_{\Omega} \frac{1}{RT} (\sigma : \nabla u + \nabla \cdot (k \nabla T)) d\Omega \quad (33)$$

where $\sigma : \nabla u = \sigma_{ij} \nabla_i u_j$. Using a clever trick, however, it is still possible to use the entropy variables in this case to compute the error associated to the Oswatitsch drag [23].

3.4 Three-dimensional inviscid flow

The extension to three dimensions poses no significant complications. In the shocked case, the shock is now a surface which, for the sake of the analysis, will be taken to be a single sheet attached to the wing surface along a curve σ_s and with an additional boundary curve σ_o along which the shock merges with the remaining smooth flow.

It can be shown that the adjoint state is still continuous across the shock, where it obeys the following shock equations

$$\begin{aligned} \nabla_{ig} \psi^T \cdot [\vec{F}]_{\Sigma} &= 0 \quad \text{on } \Sigma \\ \psi^T [\vec{F} \cdot \hat{n}_{\sigma_s}]_{\sigma_s} &= 0 \quad \text{on } \sigma_s \end{aligned} \quad (34)$$

In (34), $[\]_{\sigma_s}$ is the jump across the shock at the shock root, ∇_{ig} is the tangent gradient (the covariant derivative on Σ) and \hat{n}_{σ_s} is the normal vector to the shock boundary curve σ_s which is tangent to the shock surface.

4. Numerical tests

In the cases that follow, the flow and adjoint computations have been carried out with DLR's unstructured, finite volume solver TAU [33] using a cell-vertex, second-order, central discretization with JST scalar dissipation [34]. The near-field drag and Oswatitsch adjoint solutions are computed with the same continuous adjoint solver with only minor modifications affecting the boundary conditions. In both cases, the following adjoint boundary conditions

$$\begin{aligned} \vec{\varphi} \cdot \hat{n} &= \vec{f} \cdot \hat{n} \quad \text{on } S_w \\ \chi^T (\vec{F}_U \cdot \hat{n}) &= 0 \quad \text{along outgoing characteristics on } S_{\infty} \end{aligned}$$

are weakly enforced, with $\chi = \psi$ and \vec{f} equal to the force direction for drag/lift adjoints, and $\chi = \psi - v$ and $\vec{f} = 0$ for the Oswatitsch adjoint.

4.2 2D inviscid flow

The first example is inviscid, subcritical flow over a NACA 0012 airfoil with free-stream Mach number $M_{\infty} = 0.5$ and angle of attack $\alpha = 2^\circ$. We use this case, which was addressed in detail in [23], for validation and to confirm the equivalence between the entropy variables and the Oswatitsch adjoint variables. This is done in Figure 4, showing a good agreement which confirms that, as in the quasi-1D case, the entropy variables are dual to the Oswatitsch functional.

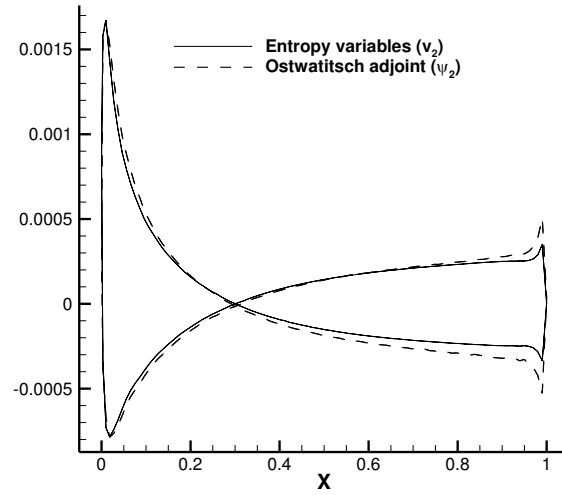


Figure 4: NACA0012 ($M_\infty = 0.5$, $\alpha = 2^\circ$). Entropy variables and Oswatitsch adjoint on the airfoil surface.

Next, we consider transonic flow past a NACA0012 airfoil with $M_\infty = 0.8$ and $\alpha = 1.25^\circ$, resulting in a strong shock at 65% chord on the suction side of the airfoil. To this setup we apply adjoint-based adaptation schemes built on the near-field drag adjoint (1), the Oswatitsch adjoint and likewise the entropy adjoint (using the entropy variables as an adjoint solution). The initial mesh, which is shown in Figure 5, has 2995 nodes, with the far-field located at approximately 50 chord-lengths away from the airfoil. Mesh adaptation is carried out by splitting in half the mesh edges according to the value of Dwight's dissipation-based local mesh adaptation indicator [35]

$$\eta_i = \left| \psi^T \left(k_2^i \frac{\partial R^{(diss)}}{\partial k_2^i} + k_4^i \frac{\partial R^{(diss)}}{\partial k_4^i} \right) \right| \quad (35)$$

where $R^{(diss)}$ is the dissipation part of the JST residual and k_2^i and k_4^i are local values of the dissipation coefficients. An edge is marked for refinement if the value of the indicator exceeds a threshold that is set implicitly by requiring that the percentage of new points introduced is fixed at 40%. When edges are split on the airfoil's surface, the position of the new points is adjusted using cubic splines reconstruction to conform to the original geometry.

Figure 5 shows the convergence of the drag coefficient for the different adaptive strategies, including isotropic refinement (where every mesh edge is split in half) for reference purposes. Errors are computed with respect to a reference value obtained by Richardson extrapolation from the isotropic refinement values. It is clear that both drag-adjoint-based approaches yield nearly identical results (and perform consistently better than the entropy adjoint) in terms of the drag coefficient (computed by pressure wall integration (1)).

The above behavior is reflected in the adapted meshes, which are shown in Figure 6. Drag-based and Oswatitsch adjoint adapted meshes show similar trends (with the Oswatitsch adjoint seemingly targeting the wake somewhat more intensely), including intense refinement along the incoming stagnation streamline and the contour of the supersonic bubble on the suction side of the airfoil, which are typical features of adjoint-adapted meshes. The entropy adjoint approach, on the other hand, targets strongly the wake and shock regions. This over-refinement prevents the entropy-based adaptation from properly refining the mesh to produce a more accurate drag coefficient.

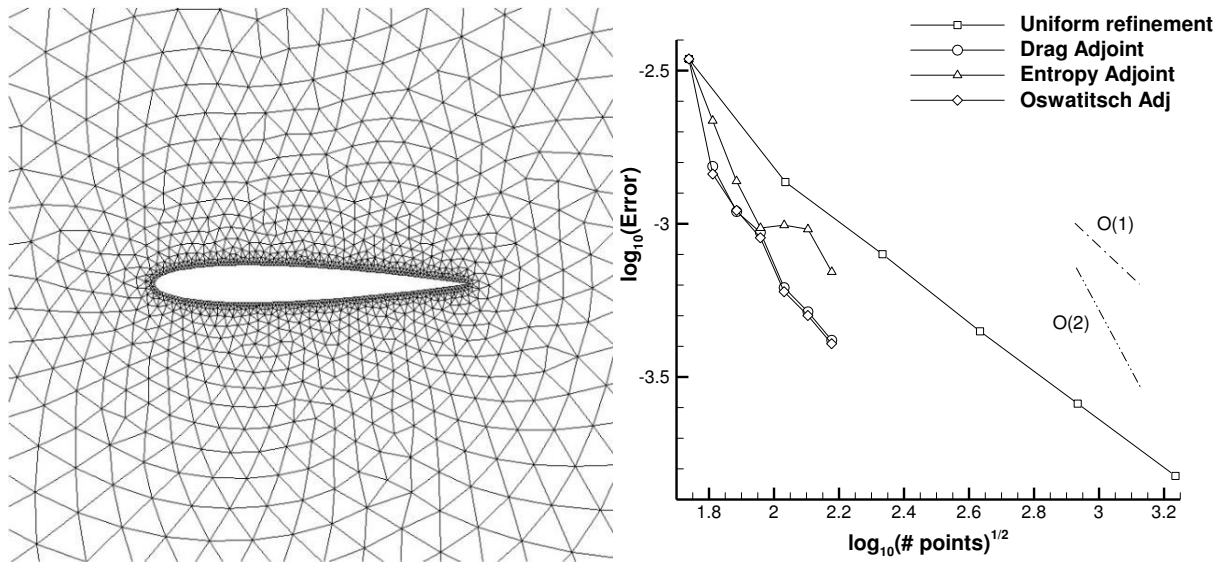
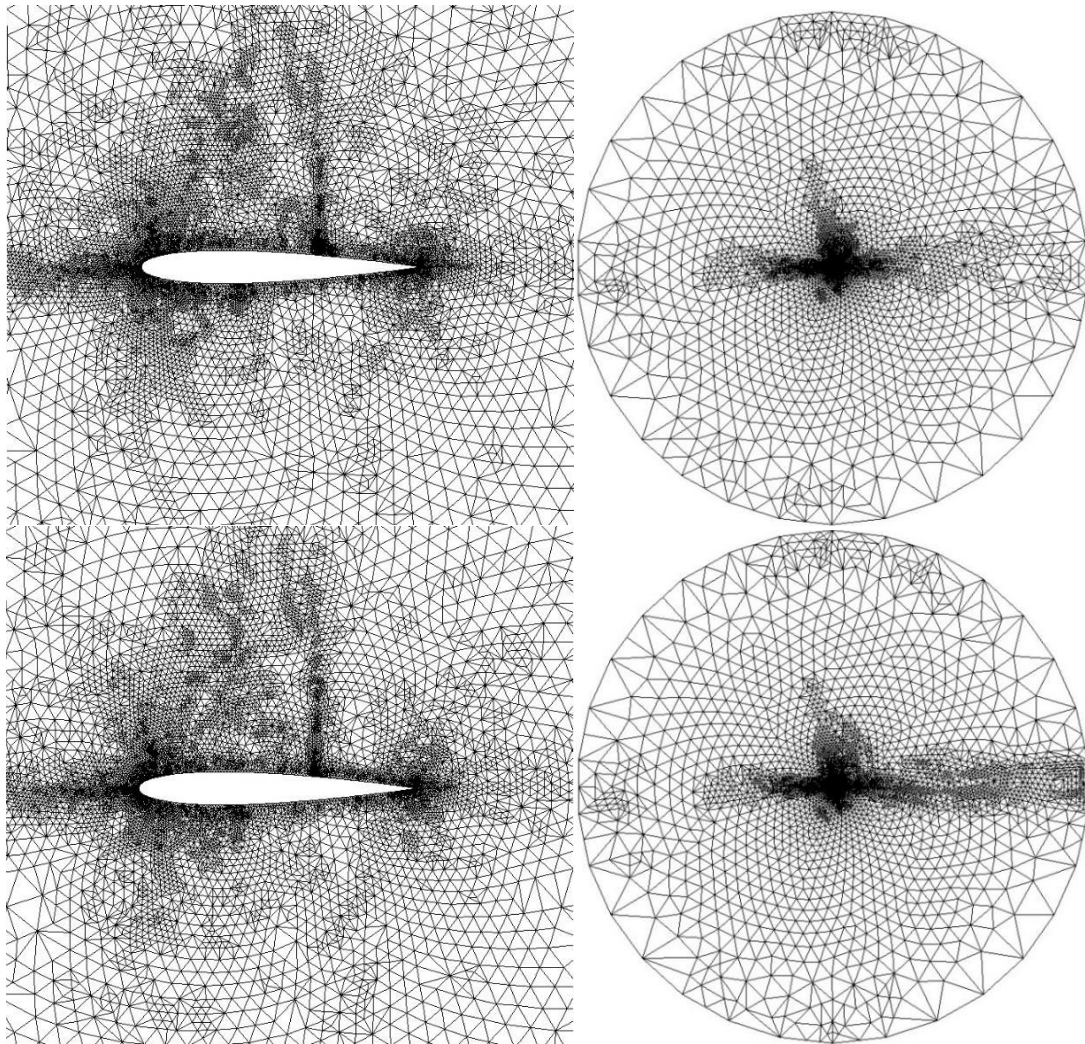


Figure 5: NACA0012 $M_\infty = 0.8$ and $\alpha = 1.25^\circ$. Initial mesh and near-field drag error convergence.



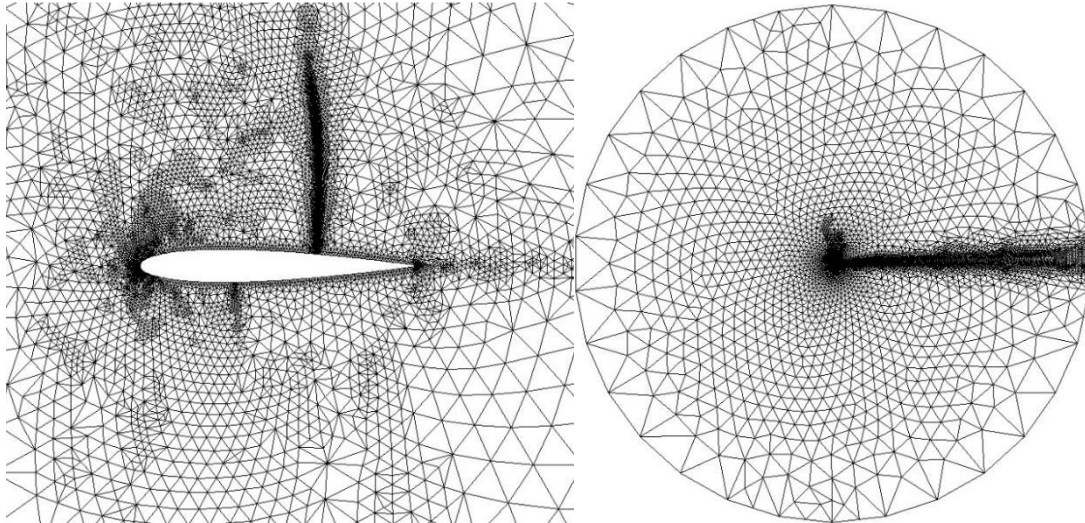


Figure 6: NACA0012 $M_\infty = 0.8$ and $\alpha = 1.25^\circ$. Final adapted meshes after 5 adaptation cycles. Top: near-field drag adjoint-based adaptation. Mid: Oswatitsch-drag-adjoint-based adaptation. Bottom: entropy adjoint.

4.3 2D viscous flow

We now examine viscous flow past a NACA 0012 airfoil with $M_\infty = 0.5$, $\alpha = 2^\circ$ and Reynolds number $Re = 5000$. The initial mesh is a hybrid, unstructured mesh with about 30 structured layers of quadrilaterals in the boundary layer. The far-field boundary is approximately 100 chord-lengths away from the airfoil.

Adjoint-based adaptation is again performed based on Dwight's indicator. Adaptation in the triangular region proceeds as explained above, while adaptation in the boundary layer proceeds by edge bisection in the streamwise (i.e., parallel to the airfoil surface) direction only.

Figure 7 shows the convergence of the near-field drag coefficient using the different adaptive strategies. We see that the Oswatitsch adaptation and the near-field drag adaptation perform comparably, and are both outperformed by the entropy adjoint approach.

The adapted meshes after 4 adaptation iterations are shown in Figure 8. Both the Oswatitsch and near-field drag adjoint approaches strongly refine the region close to the airfoil, including the wake and the incoming stagnation streamline. The Oswatitsch adjoint also targets intensely the entire wake all the way to the far-field, a feature that is shared by the entropy adjoint approach, which also targets regions of the mesh near the airfoil, as well as the portions of the wake near the airfoil but leaves the incoming stagnation streamline significantly unrefined.

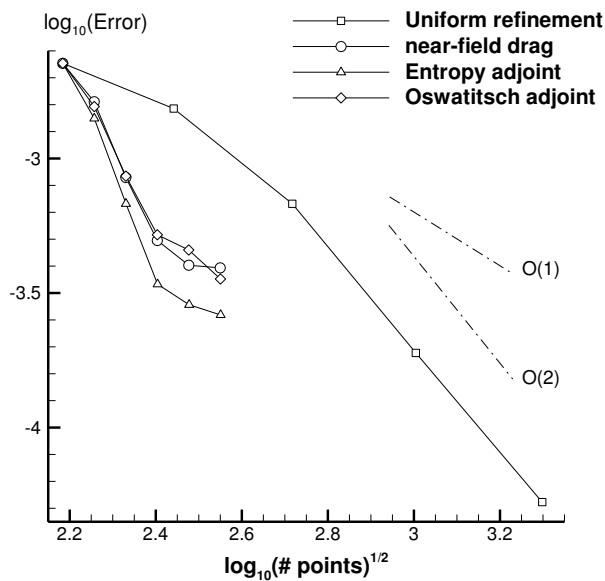


Figure 7: NACA0012 $M_\infty = 0.5$, $Re = 5000$ and $\alpha = 2^\circ$. Convergence of near-field drag

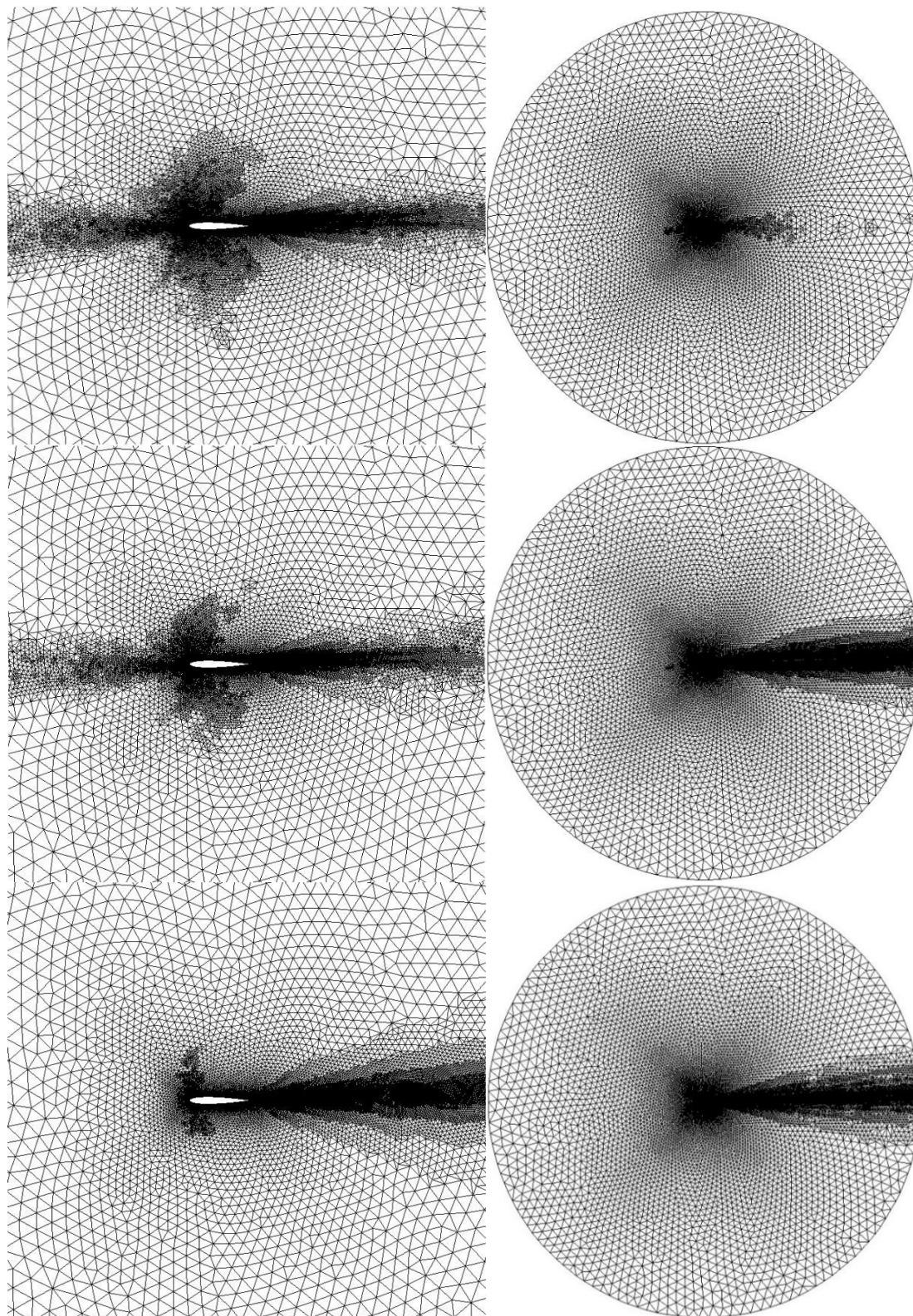


Figure 8: NACA0012 ($M_\infty = 0.5$, $Re = 5000$, $\alpha = 2^\circ$). Adapted meshes after 4 adaptation cycles. Top: near-field drag adjoint. Middle: Oswatitsch adjoint. Bottom: entropy adjoint.

4.4 3D inviscid flow

For completeness, we provide a more challenging 3D test case addressing transonic flow past an ONERA M6 wing at $\alpha = 3.06^\circ$, sideslip angle $\beta = 0^\circ$ and $M_\infty = 0.84$. The flow has a strong lambda-shaped shock on the suction side. The initial mesh consists of ~ 205000 tetrahedra and ~ 41000 nodes.

Near-field drag convergence results are shown in Figure 9. Errors are established with respect to a reference value obtained using Richardson extrapolation from computations in a sequence of globally refined meshes. The entropy adjoint approach shows error convergence, but it performs worse than uniform refinement at every stage and even worse than feature based adaptation at the earliest stages. This is likely due to the over refinement of the shock and wing-tip vortex regions that is clearly noticeable in the adapted meshes (Figure 10 and Figure 11). On the other hand, the Oswatitsch adjoint gives results comparable to the near-field drag-adjoint based scheme. This can be surprising, since in 3D the Oswatitsch formula misses a significant contribution to the drag coming from trailing vorticity (the induced drag). This should affect the drag values predicted with the formula but seems to have little influence in the adaptation process as far as prediction of near-field drag is concerned. Accordingly, the Oswatitsch adapted mesh shows a more even refinement pattern that is closer to the specific drag-based adaptation, with a slight refinement of the shock and strong refinement immediately upstream of the wing.

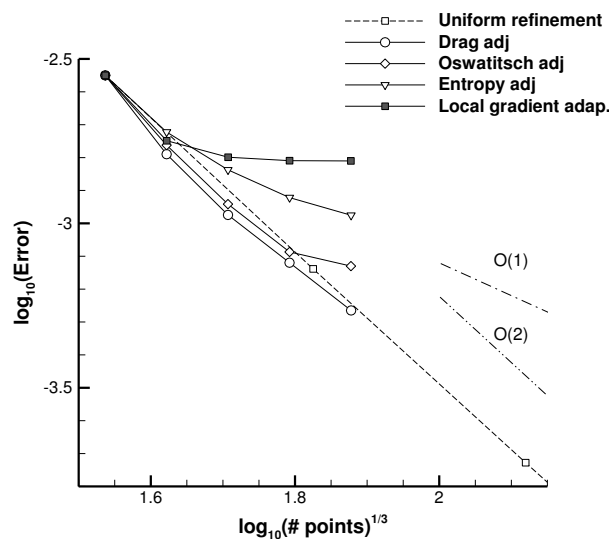


Figure 9: ONERA M6. Convergence of near-field drag for different adaptation schemes.

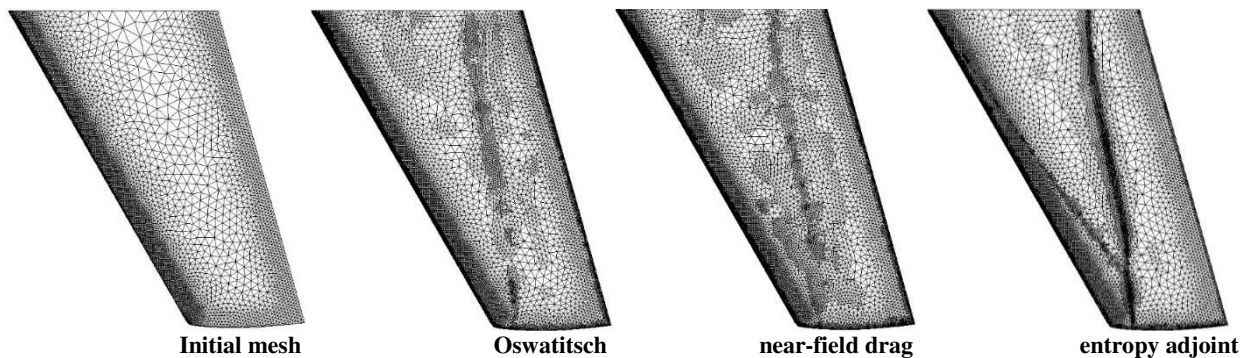


Figure 10: ONERA M6. Initial (left) and adapted surface meshes after 4 adaptation steps.

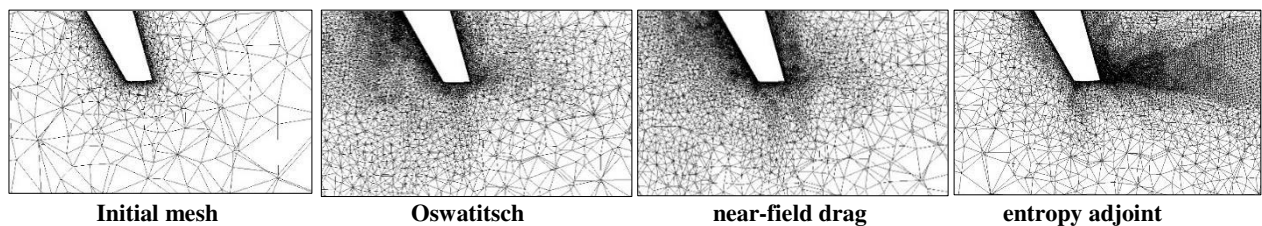


Figure 11: ONERA M6. Cut through the wing horizontal symmetry plane for the initial and adapted meshes

5. Discussion

Aerodynamic drag can be estimated by the integrated flux of entropy through domain boundaries. Following this idea, an adjoint-based mesh adaptation approach that targets the entropy flux has been investigated. For inviscid, subcritical flows, the resulting adjoint state is equivalent to the entropy variables and, thus, the approach is identical to the entropy adjoint approach of Fidkowski et al., while for shocked or viscous flows both approaches differ. In all cases, the entropy variables are related (adjoint in the inviscid case, and “quasi”-adjoint in the viscous –laminar– case) to the integrated entropy residual, which can be expressed as a global entropy balance comprising the entropy entering and leaving the domain and the entropy generated within the domain, including entropy created at shocks and boundary layers. This relates the entropy variables to spurious entropy generation, while the Oswatitsch adjoint is related to physical entropy production.

At the numerical level, on the other hand, the flow residuals weighted with the Oswatitsch adjoint target errors in the entropy flux, so they clearly include spurious entropy generation. At the same time, the residuals weighted with the entropy variables target regions of spurious entropy production (which are errors in the entropy residual) but also regions (such as shocks) of physical entropy production.

The next question is the practical application of these approaches. Both approaches have been tested in shocked inviscid 2D and 3D flows, as well as in 2D viscous flows, and compared with conventional output-based adjoint mesh adaptation. The Oswatitsch adjoint tends to mimic the drag convergence behavior of the near-field drag adjoint-based adaptation, even in 3D where the Oswatitsch formula does not account for induced drag. The adapted meshes are likewise similar, with the Oswatitsch adjoint targeting the wake more intensely than the near-field drag adjoint but avoiding the over-refinement of the shock regions that is present in both entropy-based approaches. The positive result in 2D cases may have been expected given that the Oswatitsch adjoint also targets regions of spurious entropy production which, as pointed out in [23], accounts for the difference between near-field and Oswatitsch drags.

The entropy adjoint approach, on the other hand, has the advantage of not requiring a separate adjoint solution, but it has been seen to perform worse than the drag adjoint in inviscid shocked cases. Likely, the creation of entropy at the shocks is leading to over-refinement in those regions, which may be counter-productive as far as prediction of output quantities of engineering interest is concerned. This tendency could be alleviated by weighting the sensor with cell-size dependent factors, but a more physically-based solution would be worth investigating.

The situation is different in viscous cases, at least in the subsonic, laminar case that we have analyzed, where the entropy adjoint approach has been seen to outperform the drag and Oswatitsch adjoints in terms of drag error convergence. The effect of including turbulence or viscous shocks remains to be seen.

We end with two considerations which concern the relevance of the Oswatitsch adjoint approach and the influence of the particular adaptation strategy adopted. Regarding the first issue, we explained in the introduction that the far-field evaluation of the entropy flux by itself (and not just as a surrogate for aerodynamic drag) is relevant in turbomachinery flows as a means to compute loss, which has sources other than aerodynamic drag. The adjoint formulation presented here could be of relevance in the numerical estimation of loss for these flows, as well as for optimal shape design.

Finally, the adopted adaptive strategy focuses on the elimination of artificial dissipation errors, and this should be kept in mind when assessing and extrapolating these results. However, artificial viscosity contributes significantly to spurious entropy generation, especially in inviscid flows, which supports the choice of adaptation strategy. Besides, the overall conclusions are not significantly different from what can be found in the published literature, giving more confidence in the generalizability of the results.

Acknowledgements

This work has been supported by INTA and the Spanish Ministry of Defence under the research program “Termofluidodinámica” (IGB99001). Computations have been carried out with the TAU Code, developed at DLR’s Institute of Aerodynamics and Flow Technology at Göttingen and Braunschweig, which is licensed to INTA through an R+D cooperation agreement.

References

- [1] Jameson, A. 1998. Aerodynamic design via control theory. *J. Sci. Comp.* 3(3): 233–260.
- [2] Peter, J., and R. Dwight. 2010. Numerical sensitivity analysis for aerodynamic optimization: a survey of approaches. *Comput. Fluids* 39(10):373–391.
- [3] Pierce, N., and M. Giles. 2004. Adjoint and defect error bounding and correction for functional estimates. *J. Comput. Phys.* 200(2):769–794.

- [4] Fidkowski, K., and D. Darmofal. 2011. Review of output-based error estimation and mesh adaptation in computational fluid dynamics. *AIAA J.* 49(4):673–694.
- [5] Denton, J. 1993. Loss mechanisms in turbomachines. *J. Turbomach.* 115(4):621–656.
- [6] Oswatitsch, K. 1956. Gas dynamics. Academic Press, New York.
- [7] Destarac, D. 2003. Far-field/near-field drag balance and applications of drag extraction in CFD. In: *CFD-based Aircraft Drag Prediction and Reduction*. VKI for Fluid Dynamics, Lecture Series 2003-02.
- [8] Yamazaki, W., K. Matsushima and K. Nakahashi. 2007. Drag decomposition-based adaptive mesh refinement. *J. Aircraft* 44(6):1896–1905.
- [9] Naterer, G., and J. Camberos. 2003. Entropy and the second law fluid flow and heat transfer simulation. *J. Thermophys. Heat Tr.* 17:360–371.
- [10] Puppo, G., and M. Semplice. 2011. Entropy and the numerical integration of conservation laws. In: *LSMS-2011*.
- [11] Papadimitriou, D., and K. Giannakoglou. 2006. A continuous adjoint method for the minimization of losses in cascade viscous flows. *AIAA Paper* 2006–49.
- [12] Andrews, J., and K. Morton. 1995. Spurious entropy generation as a mesh quality indicator. In: *14th International Conference on Numerical Methods in Fluid Dynamics*. Lecture Notes in Physics 453, 122–126. Springer, Berlin.
- [13] Naterer, G., and D. Rinn. 2002. Towards entropy detection of anomalous mass and momentum exchange in incompressible fluid flow. *Int. J. Num. Meth. Fluids* 39(11):1013–1036.
- [14] Puppo, G., and M. Semplice. 2011. Numerical entropy and adaptivity for finite volume schemes. *Commun. Comput. Phys.* 10(5):1132–1160.
- [15] Ching, E., and Y. Ihme. 2016. Entropy residual as a feature-based adaptation indicator for simulations of unsteady flow. *AIAA Paper* 2016–0837.
- [16] Doetsch, K., and K. Fidkowski. 2018. Combined entropy and output-based adjoint approach for mesh refinement and error estimation. *AIAA Paper* 2018–0918.
- [17] Fidkowski, K., and P. Roe. 2010. An entropy adjoint approach to mesh refinement. *SIAM J. Sci. Comput.* 32:1261–1287.
- [18] Harten, A. 1983. On the symmetric form of systems of conservation laws with entropy. *J. Comput. Phys.* 49:151–164.
- [19] Tadmor, E. 1987. Entropy functions for symmetric systems of conservation laws. *J. Math. Anal. Appl.* 122:355–359.
- [20] Lozano, C. 2014. The entropy adjoint for shocked flows: application to the quasi-1D Euler equations. DOI: 10.13140/RG.2.2.27482.54725.
- [21] Lozano, C. 2018. Singular and discontinuous solutions of the adjoint Euler equations. *AIAA J.* 56:4437–4452.
- [22] Lozano, C. 2019. Entropy and adjoint methods. *J. Sci. Comput.* (under review).
- [23] Fidkowski, K., M. Ceze and P. Roe. 2012. Entropy-based drag error estimation and mesh adaptation in two dimensions. *J. Aircraft* 49(5):1485–1496.
- [24] Giles, M., and R. Cummings. 1999. Wake integration for three-dimensional flowfield computations: Theoretical Development. *J. Aircraft* 36(2):357–365.
- [25] Giles, M., and N. Pierce. 2001. Analytic adjoint solutions for the quasi-one-dimensional Euler equations. *J. Fluid Mechanics* 426:327–345.
- [26] Anderson, J. D. 1990. Modern compressible flow, 2nd ed., p. 155. McGraw-Hill, New York.
- [27] Baeza, A., C. Castro, F. Palacios and E. Zuazua. 2009. 2-D Euler shape design on nonregular flows using adjoint Rankine-Hugoniot relations. *AIAA J.* 47(3):552–562.
- [28] Giles, M. 2003. Discrete adjoint approximations with shocks. In: *Hyperbolic Problems: Theory, Numerics, Applications*, 185–194. Springer, Berlin.
- [29] Giles, M., and N. Pierce. 1997. Adjoint equations in CFD: duality, boundary conditions and solution behavior. *AIAA Paper* 97–1850.
- [30] Anderson, W. K., and V. Venkatakrishnan. 1999. Aerodynamic design optimization on unstructured grids with a continuous adjoint formulation. *Comput. Fluids* 28:443–480.
- [31] Jameson, A., N. Pierce and L. Martinelli. 1998. Optimum aerodynamic design using the Navier-Stokes equation. *Theor. Comp. Fluid Dyn.* 10:213–237.
- [32] Castro, C., C. Lozano, F. Palacios and E. Zuazua. 2007. Systematic continuous adjoint approach to viscous aerodynamic design on unstructured grids. *AIAA J.* 45(9):2125–2139.
- [33] Schwamborn, D., T. Gerhold and R. Heinrich. 2006. The DLR TAU-code: Recent applications in research and industry. In: *Proceedings of ECCOMAS CFD 2006*. Delft University of Technology. ISBN 90-9020970-0.
- [34] Jameson, A., W. Schmidt and E. Turkel. 1981. Numerical solutions of the Euler equations by finite volume methods using Runge-Kutta time-stepping schemes. *AIAA Paper* 81–1259.
- [35] Dwight, R. 2008. Heuristic a posteriori estimation of error due to dissipation in finite volume schemes and application to mesh adaptation. *J. Comput. Phys.* 227:2845–2863.